Aalborg Universitet

Modelling of Polarized Wireless Channels Using Propagation Graphs

Adeogun, Ramoni; Pedersen, Troels

[Link to publication from Aalborg University](#)

Modelling of Polarized Wireless Channels Using Propagation Graphs
Ramoni Adeogun and Troels Pedersen

Wireless Communications Network (WCN), Department of Electronics Systems,
Fredrik Bajers Vej 7, 9220 Aalborg, Denmark
Phone: +4599408616
Email: [ra,troels]@es.aau.dk

Modelling of Polarized Wireless Channels Using Propagation Graphs

Ramoni Adeogun and Troels Pedersen

Abstract—**Simple and accurate channel models are required to evaluate the performance of multi-antenna systems with polarized antenna arrays. This paper presents a graph based model for polarized multi-antenna wireless channels by incorporating polarization diversity into the classical propagation graph based model. In addition to classical propagation effects such as attenuation, delay and phase shifts in non-polarized channel models, the proposed model incorporated antenna and scatterer based depolarization effects including polarization coupling and polarimetric responses. An illustration of the procedure for generating the transfer function and impulse response from the model is given for dual polarized channels. Simulation results show that the power delay profile exhibit exponential decay with almost equal decay rate across the co- and cross-polar channels. Our results also show that antenna orientation, relative antenna height and depolarization affect the power-delay properties of the channel.**

Index Terms—**Directed graph, polarization, MIMO system, stochastic channel model, dual polarized system**

I. INTRODUCTION

As with other wireless systems, exploiting the full benefits of polarized systems requires adequate understanding of the polarized wireless propagation channels. This is due to the fact that the underlying properties of a radio channel significantly affect the overall system performance. A common practice in design and performance evaluation of wireless communication systems is therefore, to use mathematical models for characterizing the propagation channel. In addition to temporal, frequency and directional effects in classical MIMO models, models for polarized channels must incorporate polarization and depolarization effects arising from reflections, diffractions and scattering in the propagation medium. Channel modelling for polarized MIMO systems has been the focus of active research within the last few years and a number of models have been developed based on the classical spatial channel modelling approaches for unpolarized systems (see e.g., [1], [2] and the references therein). Polarized channel models have also been defined within wireless communication projects such as 3GPP, WINNER, and COST.

The authors are with the Wireless Communications Network(WCN) Section, Department of Electronics Systems, Aalborg Unversity, Denmark

The work on polarization channel modelling has so far focused on a special case of the multi-polarized MIMO channel, i.e., MIMO systems utilizing two orthogonally polarized antennas commonly referred to as the dual polarized MIMO channel [3]. Developing generalized models for multi-polarized MIMO channel is therefore, an open problem.

Motivated by the need to study the effects of recursive and non-recursive scattering on wireless channel characterization, an alternative modelling framework based on directed propagation graph have been presented in [4]–[6]. The graph based model describes the propagation channel as a directed graph with the transmitters, receivers and scatterers as vertices and interactions between vertices defined as a time-invariant transfer function. Based on the graph description, closed-form expressions for the channel transfer function is given in [6]. The graph may be generated deterministically or following a stochastic procedure as done in the example model in [6].

Several other studies have recently presented applications and/or modifications of the graph based models to various propagation environments such as indoor [7], [8], indoor-to-outdoor [9], high speed railway [10]–[13] and millimeter wave systems [14]. Hybrid models combining the propagation graph based model with ray tracing approaches have also been studied in [15], [16]. To the best of our knowledge, there has been no study on propagation graph modelling for polarized channels.

In this contribution, we extend the propagation graph description to multiuser MIMO systems with polarized antenna and derive expressions for the transfer functions. Polarization dependent propagation characteristics including depolarization, polarization power coupling and antenna polarimetric response are incorporated into the model.

II. POLARIZED GRAPH BASED MIMO CHANNEL MODEL

In this section, we introduce the propagation graph based modelling framework in [6] and develop a generalized extension of the model to both single- and multiuser MIMO channels with multi-polarized antenna at both ends of the link.

A. Propagation Graph

The signal from a transmit antenna in a typical communication environment propagates through the channel before arriving at the receive antenna. Depending on the environment, the transmitted signal undergoes multiple interactions (reflection, diffraction and/or scattering) with objects in the propagation medium. These propagation mechanisms can be represented as a directed graph with vertices $\mathcal{V}_\mathrm{t} = \{T_1, \cdots, T_{N_\mathrm{t}}\}$, $\mathcal{V}_\mathrm{s} = \{S_1, \cdots, S_{N_\mathrm{s}}\}$ and $\mathcal{V}_\mathrm{r} = \{R_1, \cdots, R_{N_\mathrm{r}}\}$ corresponding to the transmit antennas, scatters and receive antennas, respectively. The edges of the propagation graph denote the propagation condition between the originating and terminating vertices. A propagation graph for a MU-MIMO wireless is a directed graph with N_t transmit vertices, N_s scattering vertices and N_r receive vertices. In a single user MIMO channel, N_r corresponds to the number of antenna elements on the single receiver. In a MU-MIMO case, N_r is the total number of antenna elements on all receivers. To be consistent with existing works, we denote the vertex set $\mathcal{V}$ as a union of three disjoint sets: $\mathcal{V} = \mathcal{V}_\mathrm{t} \cup \mathcal{V}_\mathrm{s} \cup \mathcal{V}_\mathrm{r}$ and the edge set $\mathcal{E}$ as a union of four disjunct sets: $\mathcal{E} = \mathcal{E}_\mathrm{d} \cup \mathcal{E}_\mathrm{t} \cup \mathcal{E}_\mathrm{s} \cup \mathcal{E}_\mathrm{r}$, where $\mathcal{E}_\mathrm{d}$ denotes the set of direct edges between transmit and receive antennas, $\mathcal{E}_\mathrm{t}$ denotes transmit to scatterer edges set, $\mathcal{E}_\mathrm{s}$ denote inter-scatterer edges and $\mathcal{E}_\mathrm{r}$ denotes scatterers to receive antennas edge set. Note that transmit and receive vertices in the directed graph are treated as sources (with only outgoing edges) and sinks (with only incoming edges), respectively. If two vertices $v_n, v_m \in \mathcal{V}$ are visible (i.e., a propagation walk or pathexists), we denote the edge between v_n and v_m as $e = (v_n, v_m)$, where n and m are the indices of the originating and terminating vertex, respectively. The originating vertex may be a transmit antenna or a scatterer and the terminating vertex is either a scatterer or receive antenna. In a polarized channel, the signal at the terminating vertex is a depolarized, attenuated, delayed and phase shifted version of the signal at the originating vertex.

B. Polarized Propagation Mechanism

In the graph representation of a polarized wireless channel, signal propagation from the transmitter to the receiver is as follows. Each transmit antenna emits a signal with multiple orthogonal components (corresponding to the different polarization components). The emitted signal components propagate through the outgoing edges of the transmit antenna. The orthogonal components arrive at the receive antenna elements via its incoming edges. The output signal at a receive antenna is therefore the sum of signals from all its incoming edges weighted by the polarimetric antenna response. A scattering vertex emits via its outgoing edges the sum of depolarized
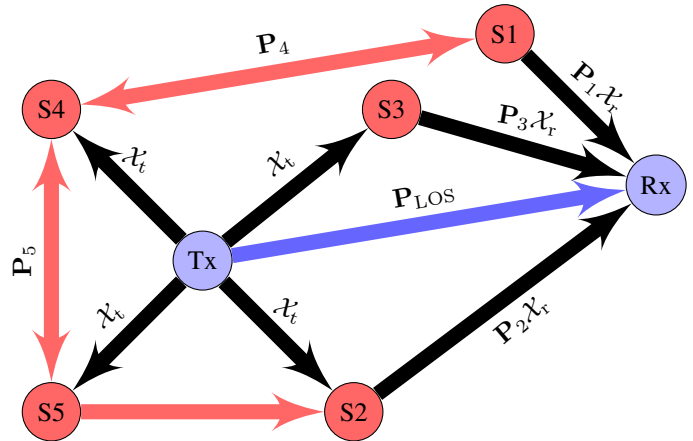

Fig. 1: a. Illustration of propagation mechanisms in a polarized graph with five scatterers.

version of all signals arriving via its incoming edges. The interaction of polarized signals with a scatterer may result in changes in the polarization state of some or all of the orthogonal components. The depolarized signals are then summed up at the scatterer and distributed to its outgoing edges. The propagation of a polarized signal via the edges in a graph and its interaction with scaterrers therefore results in attenuation, delay, phase shift and depolarization. As in [9], we assume that these propagation mechanisms are linear and time-invariant and can be represented either as a convolution with the impulse response in the time domain or a multiplication with a transfer function in the frequency domain.

C. Coordinate System and Polarization State Representation

Characterization of a wireless channel using propagation graphs may be achieved either by defining the graph structure through the vertex and edge properties or generating the adjacency matrix in a pure stochastic manner. The former involve defining the location of vertices and edge directions in a deterministic manner using knowledge of the propagation environment or following a statistical approach as presented in Section III. In this work, we utilize an earth-related, global Cartesian coordinate system where the vertical (z-axis) corresponds to the zenith and the horizontal axes (x- and y-axis) are parallel to the ground. The location of a vertex, v_n, is represented by the position vector, $\mathbf{r}_n = [x_n, y_n, z_n]^T$. We define for edge, $e = (v_n, v_m)$, the propagation direction represented by the unit vector, $\Omega_e = (\mathbf{r}_m - \mathbf{r}_n)/||\mathbf{r}_m - \mathbf{r}_n||$ which has elevation angle θ_e and azimuth angle, ϕ_e.

We define, without loss of generality, polarization states of a signal, $\mathbf{s}$, propagating through the graph by

a three-dimensional vector. For example, the signal on edge, e, is denoted as

$$\mathbf{s}_e = \begin{bmatrix} s_e^x & s_e^y & s_e^z \end{bmatrix}^T, \tag{1}$$

where $\mathbf{s}_e^x$, $\mathbf{s}_e^y$ and $\mathbf{s}_e^z$ denote the components of the signal in the three orthogonal polarization states. A three-dimensional basis has been proposed in [17] for the far field polarimetric antenna pattern representation. Other bases such as the two-dimensional *Jones* vector representation can also be used to describe the polarization states.

D. Graph Description of Polarized Propagation

Consider a polarized multi-user MIMO systems with a N_t transmit antennas and a total of N_r receive antennas. Let the vertices in the graph be indexed according to

$$v_n \in \begin{cases} \mathcal{V}_t; & n = 1, \ldots, N_t \\ \mathcal{V}_r; & n = N_t + 1, \ldots, N_t + N_r \\ \mathcal{V}_s; & n = N_t + N_t + 1, \ldots, N_t + N_r + N_s \end{cases} \tag{2}$$

The polarization state representation in (1) implies that the signal observed at every scattering vertices in the graph is a three-dimensional vector. Using the vertex indexing in (2), the propagation graph for the polarized channel can be represented by a $(N_t + N_r + 3N_s) \times (N_t + N_r + 3N_s)$ adjacency matrix,

$$\mathbf{A}(f) = \begin{bmatrix} \mathbf{0} & \mathbf{0} & \mathbf{0} \\ \mathbf{D}(f) & \mathbf{0} & \mathbf{R}(f) \\ \mathbf{T}(f) & \mathbf{0} & \mathbf{B}(f) \end{bmatrix}, \tag{3}$$

where the sub-matrices contain transfer functions:

- $\mathbf{D}(f) \in \mathbb{C}^{N_r \times N_t}$ contains the transfer function of the direct edges between all transmit and receive antenna pairs including the antenna response.
- $\mathbf{T}(f) \in \mathbb{C}^{3N_s \times N_t}$ contains the 3×1 transfer function vectors for all the $N_t N_s$ transmit antenna to scatterer edges.
- $\mathbf{R}(f) \in \mathbb{C}^{N_r \times 3N_s}$ contains the 3×1 transfer function vectors for all the $N_r N_s$ scatterer to receive antenna edges.
- $\mathbf{B}(f) \in \mathbb{C}^{3N_s \times 3N_s}$ contains the 3×3 transfer function sub-matrices for all the $N_s N_s$ scatterer to scatterer edges.
- $\mathbf{0}$ is an all-zero matrix with the appropriate dimension.

As observed in [6], the structure of $\mathbf{A}(f)$ is a consequence of the structure of the propagation graph. The first N_t rows are zeros because the transmit antennas are considered pure sources. Similarly, the $N_t + 1$ to $N_t + N_r$-th columns are zeros because receive antennas are treated as pure sinks. It should be noted that although the (3) has the same structure as given in [6] for the uni-polarized channel, the dimension and structure of the polarized submatrices differs from those in [6]. We would also like to note that extension of the model to polarized channels as presented in the following section is non-trivial.

E. Models for Gains and Polarimetric Scattering Matrix

Based on the physical propagation mechanisms in a polarized channel, the transfer function of the edge, e can be expressed as

$$\mathbf{A}_e(f) = \mathbf{G}_e(f) \odot \exp[j(2\pi\tau_e f \mathbf{1} + \mathbf{\Psi}_e)], \tag{4}$$

where $\odot$ and $\exp[.]$ denote entry-wise multiplication and entry-wise exponential, respectively. The edge propagation delay can be calculated for edge, $e = (v_n, v_m)$ from the vertex position vectors as $\tau_e = |(\mathbf{r}_m - \mathbf{r}_n)|/c$, where c is the speed of light in free space. The random phase rotations for each of the polarization components are contained in $\mathbf{\Psi}_e$, which is a 3×1 vector or 3×3 matrix. The edge gain, g_e can be calculated from

$$\mathbf{G}_e(f) = \begin{cases} \dfrac{\mathbf{F}_e}{\sqrt{(4\pi f \tau_e)^2}}; & e \in \mathcal{E}_d \\ \dfrac{\mathbf{F}_e}{\sqrt{4\pi \tau_e^2 f \mu(\mathcal{E}_t)\mathcal{S}(\mathcal{E}_t)}}; & e \in \mathcal{E}_t \\ \dfrac{g\mathbf{F}_e}{\text{odi}(e)}; & e \in \mathcal{E}_s \\ \dfrac{\mathbf{F}_e}{\sqrt{4\pi \tau_e^2 f \mu(\mathcal{E}_r)\mathcal{S}(\mathcal{E}_r)}}; & e \in \mathcal{E}_r \end{cases}, \tag{5}$$

where $|.|$ denotes the cardinality of the associated set. Here, $\text{odi}(e)$ denotes the number of outgoing edges from the nth scatterer,

$$\mu(\mathcal{E}_a) = \frac{1}{|\mathcal{E}_a|} \sum_{e \subset \mathcal{E}_a} \tau_e, \quad \mathcal{S}(\mathcal{E}_a) = \sum_{e \subset \mathcal{E}_a} \tau_e^{-2}, \quad \mathcal{E}_a \subset \mathcal{E}, \tag{6}$$

and the entity $\mathbf{F}_e$ is a matrix that captures the polarization dependent power coupling. The dimension and models for $\mathbf{F}_e$ depend on the type of edge.

1) Direct Edges: Signals propagating on a direct edge experiences two polarization dependent effects viz: array response processing at both the transmitter and receiver. Thus, $\mathbf{F}_e$ can be expressed as

$$\mathbf{F}_e = \mathcal{X}_t^T(\Omega_e)\mathcal{X}_r(\Omega_e), \quad e \in \mathcal{E}_d, \tag{7}$$

where $\mathcal{X}_t(\Omega_e)$ and $\mathcal{X}_r(\Omega_e)$ are the 3×1 transmit and receive polarimetric array response vectors, respectively. Here, $\mathbf{F}_e$ is a scalar.

2) Transmitter to Scatterer Edges: On a transmitter to scatterer edge, the polarization related effects experienced by a signal is due to the polarimetric array response processing. The polarimetric vector can therefore be obtained from

$$\mathbf{F}_e = \mathcal{X}_t(\Omega_e), \quad e \in \mathcal{E}_t. \tag{8}$$

Thus, in this case, $\mathbf{F}_e$ has dimension 3×1.

3) Scatterer to Scatterer Edges: The polarization dependent effects on a scatterer to scatterer edge include scatterer based depolarization and polarization rotation due to change in propagation direction. For simplicity reasons, we assume that all scatterers are isotropic so that polarization changes occur at the scattering interface independent of incoming and outgoing edge direction. With the 3-dimensional representation in (1), the change in the polarization states of a propagating signal due to interaction with a scatterer at vertex, v_n can be represented by a 3×3 polarization mixing matrix, $\mathbf{P}_n$ containing the co- and cross-polar power coupling between the polarization states. Assuming that the polarization dependent effect of a scatterer to scatterer edge, $e = (v_n, v_m)$, is only due to the incoming vertex (effect due to the outgoing scattering vertex is accounted for in the scatterer to receiver edge or a scatterer to scatterer edge to which the vertex is connected), $\mathbf{F}_e$ is given by

$$\mathbf{F}_e = \mathbf{P}_n, \quad e \in \mathcal{E}_s. \tag{9}$$

4) Scatterer to Receiver Edges: On a scatterer to receiver edge, the polarization mechanism include polarization mixing due to the originating vertex and array response processing due to the receive vertex, the polarization dependent vector can therefore be written as

$$\mathbf{F}_e = \mathbf{P}_n \mathcal{X}_r(\Omega_e), \quad e \in \mathcal{E}_r. \tag{10}$$

F. Transfer Function for Polarized Channel

Since all vertices in the propagation graph are fixed, the MIMO channel can be assumed to be linear and time-invariant. The signal received at the receive vertices can therefore be expressed as

$$\mathbf{Y}(f) = \mathbf{H}(f)\mathbf{X}(f), \tag{11}$$

where $\mathbf{H}(f)$ is the $N_r \times N_t$ complex transfer matrix of the propagation graph. $\mathbf{X}(f)$ and $\mathbf{Y}(f)$ are the N_t- and N_r-dimensional signals at the transmit and receive signal vertices. Using (9), the signal observed at the output of scatterer v can be written as

$$\mathbf{Z}_v(f) = \mathbf{P}_v \sum_{v' \in \mathcal{V}_s} \mathbf{Z}_{(v',v)}^{in}(f), \tag{12}$$

where $\mathbf{Z}_{(v',v)}^{in}(f) \in \mathbb{C}^{3 \times 1}$ denote the signal on edge, $e = (v', v)$. Equation (12) implies that the signal at the output of a scattering vertex is a depolarized version of the sum of signals on all incoming edges of the vertex. This is reasonable since scatterers are assumed to be isotropic such that depolarization is independent of propagation directions. The signals observed at the scatterers can now be collected into the $3N_s \times 1$ vector,

$$\mathbf{Z}(f) = [\mathbf{Z}_1^T(f), \dots, \mathbf{Z}_{N_s}^T(f)]^T. \tag{13}$$
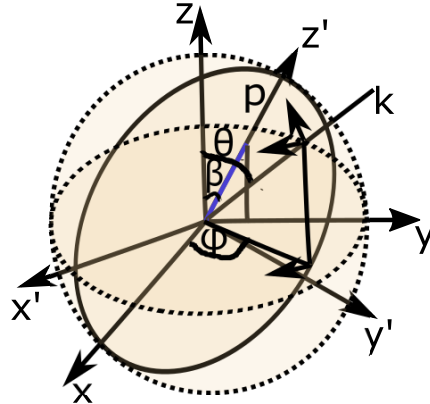

Fig. 2: 3D coordinate system

Using the vertex indexing in (2), the signals at all vertices can be collected into the $N_t + N_r + 3N_s$ dimensional vector,

$$\mathbf{C}(f) = [\mathbf{X}(f)^T, \mathbf{Y}(f)^T, \mathbf{Z}(f)^T]^T. \tag{14}$$

Using (14) and following a similar procedure as in [5], [6], the transfer function for the dual polarized channel is obtained as

$$\begin{aligned} \mathbf{H}(f) &= \mathbf{D}(f) + \mathbf{R}(f)[\mathbf{I} + \mathbf{B}(f) \\ &\quad + \mathbf{B}^2(f) + \cdots + \mathbf{B}^n(f) + \dots]\mathbf{T}(f) \\ &= \mathbf{D}(f) + \mathbf{R}(f)[\mathbf{I} - \mathbf{B}(f)]^{-1}\mathbf{T}(f). \end{aligned} \tag{15}$$

As discussed in [6], a necessary and sufficient condition for the closed form channel transfer function expression in (15) is that the spectral radius of $\mathbf{B}(f)$ be less than unity.

III. Generation of Polarized Graph Model: Application to Dual Polarized MIMO Systems

In this section, we apply the generalized model to a specific type of polarized system. We consider dual polarized MIMO configurations in recent wireless standards where the antenna array at both ends are composed of pairs of collocated orthogonally polarized half-wave dipole antennas (see e.g., [3]). In dual polarized MIMO modelling literature, the propagating signal is often decomposed into vertically polarized (V) and horizontally polarized (H) components. An alternative representation which is used in this paper is the polar-spherical polarization basis which decomposes the polarized signal into $\hat{\theta}$- and $\hat{\phi}$-polarized components corresponding to the vertical and horizontal polarization.

A. Polarimetric Antenna Pattern

Let the half-wave dipole antenna be oriented in the y-z plane at a tilt angle, β, to the z-axis as shown in Fig. 2.

We denote unit vectors along the antenna orientation and propagation direction as $\hat{\mathbf{p}}$ and $\hat{\mathbf{k}}$, respectively. The direction vector, $\hat{\mathbf{k}} = [\sin\theta\cos\phi, \sin\theta\sin\phi, \cos\theta]$ is perpendicular to both vertical and horizontal polarization directions as shown in Fig. 2. Using the coordinates defined in Fig. 2, unit vectors, $\hat{\mathbf{p}}$, $\hat{\theta}$ and $\hat{\phi}$ are obtained as

$$\hat{\mathbf{p}} = [0 \ \sin\beta \ \cos\beta]$$
$$\hat{\theta} = [\cos\theta\cos\phi \ \cos\theta\sin\phi \ \sin\theta]$$
$$\hat{\phi} = [\sin\phi \ \cos\phi \ 0]. \quad (16)$$

The array response in the vertical and horizontal polarization directions can therefore be expressed as

$$\begin{bmatrix} \mathcal{X}^{\hat{\theta}} \\ \mathcal{X}^{\hat{\phi}} \end{bmatrix} = \begin{bmatrix} \hat{\theta} \\ \hat{\phi} \end{bmatrix} \hat{\mathbf{p}}^T \exp(j\hat{\mathbf{k}}\bar{\mathbf{r}})$$
$$= \begin{bmatrix} \cos\beta\sin\theta + \sin\beta\cos\theta\sin\phi \\ \sin\beta\cos\phi \end{bmatrix} \exp(j\hat{\mathbf{k}}\bar{\mathbf{r}}), \quad (17)$$

where $\mathbf{k} = 2\pi/\lambda[\sin\theta\cos\phi \ \sin\theta\sin\phi \ \cos\theta]$ is the wave-vector with wavelength, λ and $\mathbf{r}$ denotes the location vector. Similar expression have been used for 3D antenna response in [2], [18]. It should be noted that the array response in 2D (without propagation in elevation plane) is a special case of (17) with $\theta = \pi/2$ and $\hat{\theta} = [0 \ 0 \ 1]$. With an inclination angle of $\beta = 0^o$ in (17), the antenna response has only vertical component. However, at other tilt angles, both vertical and horizontal components are non-zero.

B. Transfer Function Generation

We assume that the position of all vertices lie in a bounded region, representing a rectangular room. The transmitter and receiver locations are assumed to be fixed and known and scatterer positions are drawn randomly from a uniform distribution over the bounded region. An edge $e \in \mathcal{E}$ is drawn with probability

$$\Pr[e \in \mathcal{E}] = \begin{cases} P_{\mathrm{dir}}, & e \in \mathcal{E}_{\mathrm{d}} \\ P_{\mathrm{vis}}, & e \in (\mathcal{E}_{\mathrm{t}}, \mathcal{E}_{\mathrm{s}}, \mathcal{E}_{\mathrm{r}}) . \\ 0, & \text{otherwise} \end{cases} \quad (18)$$

The edge directions as well as azimuth and elevation angles are estimated using the vertex positions. The array response vector is then computed using (15) for all transmitter to scatterer and scatterer to receiver edges. The polarimetric phases $\mathbf{\Psi}_e : e \in \mathcal{E}$ are drawn from a uniform distribution on $[0, 2\pi)$ and polarimetric edge gains are computed using (5). Based on these parameters of the graph, entries of the graph adjacency matrix are computed using (4). The polarized channel transfer function is estimated over the desired frequency range,

TABLE I: Parameters for the Dual Polarized MIMO Example

Parameter	Symbol	Default Value
Antenna		2×2
Room size		$[0, 5.0] \times [0, 5.0] \times [0, 2.5]\,\mathrm{m}^3$
Transmitter position		$[1.8, 2.0, 2.0]^T\,\mathrm{m}$
Receiver position I		$[1.8, 3.4, 2.0]^T\,\mathrm{m}$
Receiver position II		$[1.8, 3.4, 0.5]^T\,\mathrm{m}$
Number of Scatterers	N_{s}	10
Prob. of direct edge	P_{dir}	1
Prob. of visibility	P_{vis}	0.92
Reflection gain	g	0.8
Frequency range		$[2, 3]\,\mathrm{GHz}$
Sampling rate		$5\,\mathrm{MHz}$
Pol. mixing param.	γ	0.2
Window		Hann

$[f_{\min}, f_{\max}]$ from (15). The time domain channel impulse response of the polarized channel is then obtained via a windowed inverse Fourier transform of the transfer function.
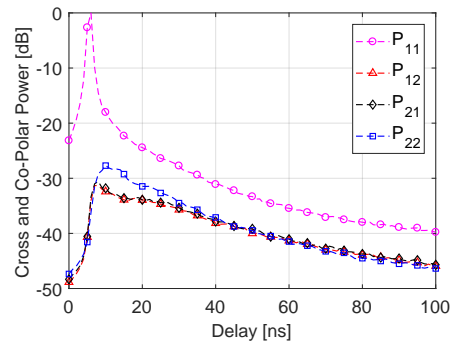

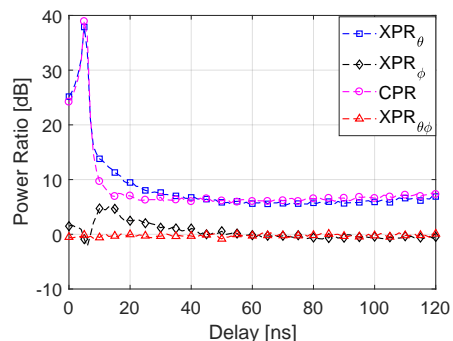Fig. 3: PDP for $0/90^o$ MIMO channel. Receiver at Location I.

Fig. 4: Power Ratios for $0/90^o$ MIMO channel. Receiver at Location I.

IV. SIMULATIONS AND RESULTS

In this section, we study the effects of recursive scattering and scatter based depolarization on the power-delay properties of dual polarized MIMO channel. We perform 1000 Monte
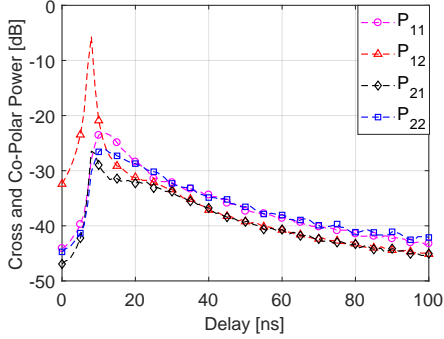
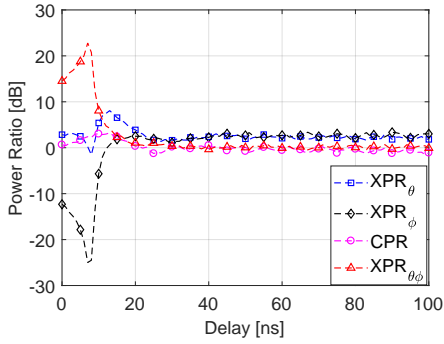Fig. 5: Co and Cross-Polar Power for $\pm 45^o$ MIMO channel. Receiver at Location II.

Fig. 6: Power Ratios for $\pm 45^o$ MIMO channel. Receiver at Location II.

Carlo simulation runs with the simulation parameters shown in Table I. We consider four co- and cross-polarization ratios:

$$\text{XPR}_\theta = \frac{\text{P}_{\theta\theta}}{\text{P}_{\phi\theta}}; \ \text{XPR}_\phi = \frac{\text{P}_{\phi\phi}}{\text{P}_{\theta\phi}}; \ \text{CPR} = \frac{\text{P}_{\theta\theta}}{\text{P}_{\phi\phi}}; \ \text{XPR}_{\theta\phi} = \frac{\text{P}_{\theta\phi}}{\text{P}_{\phi\theta}}$$

where $\text{P}_{ab} = \mathbb{E}[|h_{ab}|^2]$ denotes the average power of the channel between the b- and a- polarization at the transmitter and receiver, respectively. The terms XPR_θ and XPR_ϕ are the cross-polar ratios (ratio of co-channel power to cross channel power) for the θ- and ϕ-polarization components, respectively. CPR represents the co-polar ratio - ratio of the two co-channel powers. The last metric denoted $\text{XPR}_{\theta\phi}$ provides a measure for comparison between leakages from one polarization component
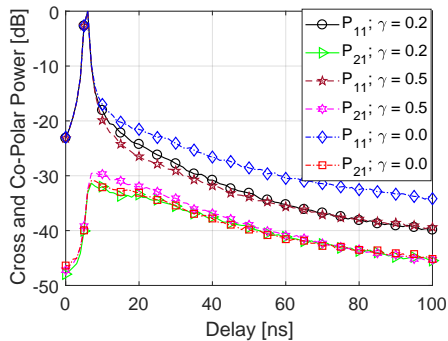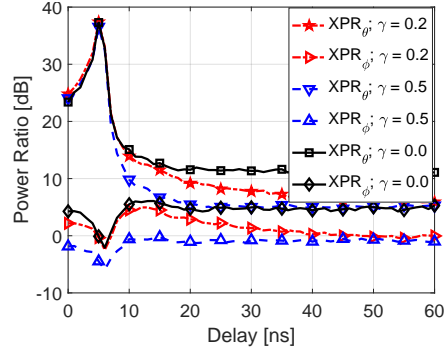

Fig. 7: Effects of mixing parameter on PDP.

Fig. 8: Effects of mixing parameter on power ratio.

to the other. We model the coupling matrix, $\mathbf{P}_n$, as

$$\mathbf{P}_n = \begin{bmatrix} 1-\gamma_n & \gamma_n \\ \gamma_n & 1-\gamma_n \end{bmatrix}, \tag{19}$$

where $\gamma_n \in [0,1)$ denotes the ratio of the power that is leaked from one polarization to the other during interaction with a scatterer.

Fig. 3 shows that the power delay profile (PDP) for all co- and cross- channels decay exponentially with the vertical to vertical channel (i.e.,P_{11}) having the strongest power over the entire delay values. A plausible explanation for this power difference is the variation in the array responses with different antenna orientation. The figure also shows that the co- and cross-polar channels exhibit slightly different decay rates for the early interactions/delays with no significant difference in decay rate for subsequent interactions. This can be seen more clearly in the power ratio plots in Fig. 4 where the power ratios vary for delays up to 30 ns and remain approximately constant afterwards. This trend in power ratios represent a transition from a state where the channels are polarized to a partially polarized or an un-polarized state. Similar results were obtained for the $0/90^o$ configuration with the receiver at location II except that all the co- and cross- channels has direct path contributions (though with different powers). As seen in Fig. 3, only the channel between transmit and receive antennas oriented at $\beta = 0^o$ has a direct component. This is expected since both vertical (θ-pol) and horizontal (ϕ-pol) polarization components of a horizontally (i.e., $\beta = 90^o$) oriented antenna become nulled out with equal antenna heights.

Fig. 5 shows that PDP for the $\pm 45^o$ configuration with the receiver at location II also decay exponentially with a direct component only visible in the -45° to $+45^o$ cross channel. In addition, we observe that the co- and cross-polar channels has nearly equal power for all non line-of-sight contributions with arrival times greater than or equal to approximately 20 ns. This is intuitive since the array response for both $+45^o$ and -45° oriented dipole has similar radiation gain in all directions. Similar effect of the radiation pattern is also observed with the receiver at location I. The power ratios plot for the $\pm 45^o$ configuration in Fig. 6 also exhibit transitions from varying ratios for early interactions (polarized) to constant power ratios for subsequent interactions (depolarized).

Finally, we illustrate the effects of varying polarization mixing parameter, γ, on the PDP in Fig. 7. We observed that increasing the mixing parameter results in a decrease in the power of the co-polar channels and increase in the power of the cross-polar channels. This is intuitive since more power is expected to be leaked from the co- to cross-polar channels with

an increase in mixing ratio. The power ratio plots in Fig. 8 also decrease with increasing mixing parameter.

V. CONCLUSION

This paper presented a generalized propagation graph based model for multi-polarized MIMO wireless channels. An illustrative application to dual polarized indoor MIMO channels is also given. Our results indicate that the power delay profile of the co- and cross- polar channels decay exponentially with approximately equal decay rates. A transition from polarized to depolarized state is observed in the power ratios. It is also seen that antenna orientation and height, and polarization coupling parameter affect the power-delay characteristics of the channel. Future research will investigate methods for modelling the per scatterer mixing parameter and compare the model with measurements.

ACKNOWLEDGMENT

REFERENCES

[1] X. Su, D. Choi, X. Liu, and B. Peng, "Channel model for polarized mimo systems with power radiation pattern concern," *IEEE Access*, vol. 4, pp. 1061–1072, 2016.

[2] M. Shafi, M. Zhang, A. L. Moustakas, P. J. Smith, A. F. Molisch, F. Tufvesson, and S. H. Simon, "Polarized mimo channels in 3-d: models, measurements and mutual information," *IEEE J. Sel. Areas Commun.*, vol. 24, no. 3, pp. 514–527, Mar 2006.

[3] Y. He, X. Cheng, and G. L. Stuber, "On polarization channel modeling," *IEEE Trans. Wireless Commun.*, vol. 23, no. 1, pp. 80–86, Feb 2016.

[4] T. Pedersen and B. H. Fleury, "A realistic radio channel model based in stochastic propagation graphs," in *5th Conf. on Mathematical Modelling (MATHMOD 2006)*, Feb. 2006, pp. 324–331.

[5] ——, "Radio channel modelling using stochastic propagation graphs," in *IEEE ICC*, June 2007, pp. 2733–2738.

[6] T. Pedersen, G. Steinbock, and B. H. Fleury, "Modeling of reverberant radio channels using propagation graphs," *IEEE Trans. Antennas Propag.*, vol. 60, no. 12, pp. 5978–5988, Dec 2012.

[7] R. Zhang, X. Lu, Z. Zhong, and L. Cai, *A Study on Spatial-temporal Dynamics Properties of Indoor Wireless Channels*, 2011, pp. 410–421.

[8] B. Uguen, N. Amiot, and M. Laaraiedh, "Exploiting the graph description of indoor layout for ray persistency modeling in moving channel," in *EUCAP*, Mar 2012, pp. 30–34.

[9] T. Pedersen, G. Steinbock, and B. H. Fleury, "Modeling of outdoor-to-indoor radio channels via propagation graphs," in *URSI General Assembly and Scientific Symposium*, Aug 2014, pp. 1–4.

[10] W. Cheng, C. Tao, L. Liu, R. Sun, and T. Zhou, "Geometrical channel characterization for high speed railway environments using propagation graphs methods," in *Intern. Conf. on Adv. Comm.n Tech.*, Feb 2014, pp. 239–243.

[11] L. Tian, V. Degli-Esposti, E. M. Vitucci, X. Yin, F. Mani, and S. X. Lu, "Semi-deterministic modeling of diffuse scattering component based on propagation graph theory," in *IEEE PIMRC*, Sept 2014, pp. 155–160.

[12] T. Zhou, C. Tao, S. Salous, Z. Tan, L. Liu, and L. Tian, "Graph-based stochastic model for high-speed railway cutting scenarios," *IET Microwaves, Antennas Propagation*, vol. 9, no. 15, pp. 1691–1697, 2015.

[13] D. K. Ntaikos, A. C. Iossifides, and T. V. Yioultsis, "Enhanced graph-theoretic channel model for performance evaluation of mimo antennas and millimeter wave communications," in *EuCAP*, May 2015, pp. 1–4.

[14] J. Chen, X. Yin, L. Tian, and M. D. Kim, "Millimeter-wave channel modeling based on a unified propagation graph theory," *IEEE Commun. Lett.*, vol. 21, no. 2, pp. 246–249, Feb 2017.

[15] G. Steinbck, M. Gan, P. Meissner, E. Leitinger, K. Witrisal, T. Zemen, and T. Pedersen, "Hybrid model for reverberant indoor radio channels using rays and graphs," *IEEE Trans. Antennas Propag.*, vol. 64, no. 9, pp. 4036–4048, Sept 2016.

[16] L. Tian, V. Degli-Esposti, E. M. Vitucci, and X. Yin, "Semi-deterministic radio channel modeling based on graph theory and ray-tracing," *IEEE Trans. Antennas Propag.*, vol. 64, no. 6, pp. 2475–2486, June 2016.

[17] Y. Chen and T. Simpson, "Radiation pattern analysis of arbitrary wire antennas using spherical mode expansions with vector coefficients," *IEEE Trans. Antennas Propag.*, vol. 39, no. 12, pp. 1716–1721, Dec 1991.

[18] M. T. Dao, V. A. Nguyen, Y. T. Im, S. O. Park, and G. Yoon, "3d polarized channel modeling and performance comparison of mimo antenna configurations with different polarizations," *IEEE Trans. Antennas Propag.*, vol. 59, no. 7, pp. 2672–2682, Jul 2011.